Applied Catalysis B: Environmental 231 (2018) 161–172

Contents lists available at ScienceDirect

Applied Catalysis B: Environmental

journal homepage: www.elsevier.com/locate/apcatb

Bed flow photoreactor experiments to assess the photocatalytic nitrogen oxides abatement under simulated atmospheric conditions

F. Mothes[a], S. Ifang[b], M. Gallus[b], B. Golly[c], A. Boréave[c], R. Kurtenbach[b], J. Kleffmann[b], C. George[c], H. Herrmann[a,*]

[a] Leibniz-Institute for Tropospheric Research (TROPOS), Atmospheric Chemistry Department (ACD), Permoserstraße 15, 04318 Leipzig, Germany
[b] Institute for Atmospheric & Environmental Research, Bergische Universität Wuppertal (BUW), Gaußstr. 20, 42119 Wuppertal, Germany
[c] Univ Lyon, Université Claude Bernard Lyon 1, CNRS, IRCELYON, F-69626, Villeurbanne, France

ARTICLE INFO

Keywords:
Heterogeneous photocatalysis
Titanium dioxide
Cement-based material
NO_x
Bed flow reactor

ABSTRACT

Small scale bed flow photoreactor experiments were performed to assess the photocatalytic performance of cement-based TiO_2-containing materials for NO_x reduction through the determination of kinetic parameters under variation of the experimental conditions (relative humidity, flow rate, mixing ratio and light intensity) and monitoring of potential reaction products in the gas phase and the aqueous extract of the surface.

The results clearly demonstrated the general potential of the tested material to photocatalytically remediate gas phase NO_x by conversion into nitrite and nitrate as identified reaction products at the surface. The measured uptake coefficients for NO and NO_2 under atmospheric relevant conditions were in the range of 5×10^{-5} with a corresponding surface deposition velocity of about 0.5 cm s^{-1}. However, it became also clear that the photocatalytic activity is in part significantly dependent on the experimental conditions. The relative humidity and the mixing ratio of the air pollutant were identified as the most important parameters. In addition, under certain conditions, a renoxification process can occur.

The comprehensive results of the present study are discussed in detail to develop recommendations for a possible future application of this technique to improve urban air quality.

1. Introduction

Clean air is essential to human health and for the intactness of the environment. Since the industrial revolution, however, the quality of the air that people breathe has deteriorated considerably as a result of human activities. The need to deliver cleaner air has been recognized for several decades with action having been taken at national, EU-level and world-wide levels, not at least through multilateral international conventions and activities. Despite significant reduction of pollutant emissions, serious air pollution problems still persist [1]. Against this backdrop, the EU adopted in 2013 the “New Clean Air Package”, including the update of legal monitoring of pollutant emissions by industry, transport, power plants and agricultural activities [2]. The long-term objective is to achieve levels of air pollution that do not lead to unacceptable harm to human health and the environment until 2050. EU-action has therefore focused on establishing minimum air quality standards for ambient air to tackle the problems of particulate matter (PM) and ground level ozone (O_3). In this context, nitrogen oxides (i.e., $NO_x = NO + NO_2$) play an important role, since they contribute, in combination with volatile organic compounds (VOCs), to the formation of these most problematic secondary air pollutants. Sources for NO_x are high temperature combustion processes, mainly emitted by power plants (21% by energy industry) and combustion engines (47% by the transport sector) [2]. To protect human health, the EU Air Quality Directive (EU, 2008c, Directive 2008/50/EC) introduced a threshold value for NO_2 (annual mean 40 µg m^{-3}) which is often exceeded by the accumulated car emissions at traffic hotspots in urban areas. In 2014, 94% of the measuring stations with values above the limit were traffic related [1].

Among new technical “solutions” designed for large dissemination over the public space, new photocatalytic building and coating materials have been proposed as a “green” remediation technology for NO_x and VOCs in the polluted urban environment [3,4]. These commercial products are based on the photocatalytic properties of a thin layer of the semiconductor titanium dioxide (TiO_2) deposited at the surface of the material (such as glass, pavement, etc.) or embedded in the substrate e.g., in paints or concrete and their depollution performance has already been assessed in numerous studies [5–21].

* Corresponding author.
E-mail address: herrmann@tropos.de (H. Herrmann).

https://doi.org/10.1016/j.apcatb.2018.03.010
Received 6 February 2018; Accepted 3 March 2018
Available online 04 March 2018
0926-3373/ © 2018 The Author(s). Published by Elsevier B.V. This is an open access article under the CC BY license (http://creativecommons.org/licenses/BY/4.0/).

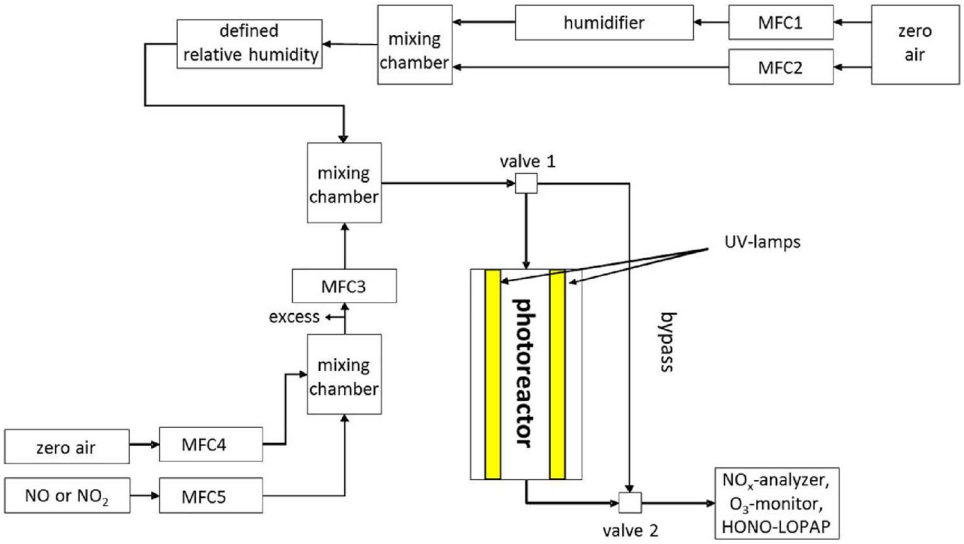

Fig. 1. Schematic overview of the experimental set-up, MFC = mass flow controller.

The interaction of the TiO_2 based photocatalyst and light of appropriate wavelength (UV-light, ≤400 nm, [22]) results in a charge separation according to Hoffmann, et al. [23]:

$$TiO_2 + h\nu \rightarrow h^+_{vb} + e^-_{cb} \qquad \text{fs range} \qquad \text{(R-1)}$$

Here, an electron from the valence band of the semiconductor is promoted into the conduction band (e_{cb}^-), leaving a hole in the valence band (h_{vb}^+). Both at the surface, or, through their diffusion through the particle bulk, both photogenerated charge carriers might recombine (null cycle) while only at the surface they can react with adsorbed reactants creating radicals. For example, the reaction with oxygen and water lead to the formation of highly reactive radicals such as O_2^-/HO_2 and OH proven by measurements using, e.g., electron paramagnetic resonance (EPR) [24], cavity ring down spectroscopy (CRDS) [25] or laser-induced fluorescence (LIF) [26–29]. These reactive oxygen species (ROS) enable irradiated TiO_2, especially in its most active form Anatase [30], to degrade adsorbed NO_x and VOCs [31,32].

Based on laboratory studies, it is generally concluded that NO_x is quantitatively converted into nitrate anions [6,11,33–35], which remain adsorbed on the surface until washed off, for example by rain, whereas the VOCs are mostly mineralized to carbon dioxide and water [36,37]. However, some recent studies on pure photocatalysts and on self-cleaning window glass also observed the formation of harmful intermediates, for example nitrous acid (HONO) [6,38,39], which is even more harmful than the primary reactants NO and NO_2. In addition, renoxification originating from adsorbed nitrate, proposed by the photocatalytic formation of the nitrate radical (NO_3) on TiO_2, was recently observed in laboratory experiments [40–44]. Both results are dependent on the material used and the applied experimental conditions, but would potentially contradict the application of photocatalytic surfaces to improve urban air quality. Accordingly, these materials are still under controversial discussion and there is an urgent need for a better characterization of such surfaces at atmospheric relevant conditions.

Therefore, the present study focuses on the reaction of NO_x with a photocatalytically active cement-based material under simulated atmospheric conditions using bed flow photoreactor experiments. Kinetics and observed products are studied under variation of the experimental conditions (carrier gas, relative humidity (RH), mixing ratio, flow rate and light intensity) and a mechanism according to the experimental results is derived. Furthermore, the obtained kinetic parameters, experimental dependencies and observed reaction products are evaluated in the context of improving urban air quality and recommendations for a future application of this technique are discussed.

2. Experimental

2.1. Sample preparation

Two different photocatalytically active cement-based coating materials prepared by the manufacturer CTG Italcementi Group (based on the TX Active® technology, [45]) have been investigated and compared with an inactive reference material (R_i), which had the same composition as the active materials but without the photocatalyst TiO_2. The photocatalytically active materials contained different amounts of TiO_2 (approximate composition: A = 0.3% and B = 1.0% wt.) and approximately 1.0 ± 0.3% of organic carbon (measuring protocol given in SI 1) as organic additive/binding material. To investigate the cement-based coating material it was mixed with ultra-pure water (Milli-Q gradient A 10, 18.2 MΩ cm, 3 ppb TOC, Millipore) using a water to solid ratio of w/s = 0.175 and subsequently applied on sand blasted glass plates (dimensions: 5 × 40 cm) with a final surface thickness of about 3-4 mm. After a curing period of approximately one month, the coated glass plates were cleaned with ultra-pure water and dried under clean air conditions to avoid a surface contamination due to adsorption of chemical compounds or dirt/dust particles from ambient air.

2.2. Experimental set-up and procedure

For the qualitative and quantitative assessment of the photocatalytic efficiency of such materials, different standard methods (UNI, ISO) request different types of small laboratory scale photoreactors. In the present study, the photocatalytic experiments were performed using small horizontal bed plugged flow reactors related to ISO 22197-1 [46]. However the experimental conditions and the data evaluation were different to ISO 22197-1, which is explained below in detail. Fig. 1 gives an overview about the experimental set-up.

Three different types of bed flow reactors were used, which slightly differed by their sizes, gas flow and light conditions, hereby ensuring that the reported data are not system dependent. The rectangular photoreactors are made out of chemically inert polytetrafluoroethylene e.g., one with a volume of 2.4×10^{-4} m^3 without any sample (dimensions 0.410 m × 0.059 m × 0.010 m). For the photocatalytic experiments, the sample plate is placed inside and the reactor is subsequently air tight closed on top with a quartz glass plate resulting in a free space of approximately 4 mm between the surface of the sample and the glass plate. This free space could be varied (2–10 mm) in order to assess the importance of diffusion limitations in the kinetics reported

below. Generally, UV-lamps, i.e. 2 BL Quantum F20 (Havells Sylvania) are placed in a light-tight cover encasing the photoreactor. However, other types of lamps were also used such as those having an emission maximum at 370 nm (Phillips TL/05, 20 W, 300–500 nm). Light intensity was measured either via an optical fiber (M26L02, Thorlabs) connected to a gated ICCD camera (PI-MAX ICCD 1024 SB 25GenII, Princeton Instruments) coupled with a grating spectrograph (Spectra Pro®-300i, Acton Research Corporation, calibration procedure explained in Mothes, et al. [44]) or a calibrated spectral radiometer (Metcon). Measured irradiance spectra are given as Supporting information (SI 2 and SI 3). By varying the distance to the sample plate, the light intensity at the surface could be varied in a range of 3–48 W m^{-2} (300–400 nm). During the experiments (except for the variation of the carrier gas), the reactor was flushed with zero air (compressed air in combination with a zero air supplier NGA19S (MCZ Umweltchemie)), or using synthetic air (5.0 from a cylinder) with a gas flow between 2-7 L min^{-1} controlled by mass flow controllers. The relative humidity (RH) was adjusted by using a controlled stream of zero air passing a humidifier tube half filled with ultra-pure water (RH 0-88%). For the experiments with NO_x, mixtures of NO (0.3 vol.-% in nitrogen, Air Liquide) and NO_2 (1% in synthetic air, Linde) were diluted with zero air to the desired starting mixing ratio, typically of atmospherically relevant 100 ppb NO/NO_2. An overview about the analytical instruments connected to the experimental set-up is given in Section 2.3.

Generally, an experiment started with a preconditioning phase, including the irradiation of the clean sample in the reactor under zero air and the desired experimental conditions (RH and flow rate) over night. After that, the photocatalytic experiment started by adding the gas phase reactant to the experimental set-up, however first via the bypass (no contact to the materials surface) to adjust the desired mixing ratio. By switching valve 1, the gas flow passes through the reactor (see Fig. 1), but first without UV-light to study any dark reaction between NO_x and the materials surface. After stable conditions are reached the UV-lamps are switched on to study the photocatalytic effect. To clearly identify the real photocatalytic influence and not to measure for example just photolysis, the results of the inactive material are always considered.

2.3. Instrumentation

For the photocatalytic experiments in the present study different analytical devices were connected to the experimental system. Unless otherwise stated, NO and NO_2 were measured using a NO_x-analyzer (APNA-370, Horiba or Modell 42i, Thermo Scientific) based on chemiluminescence detection and molybdenum converter. Additionally, ozone was determined using an ozone monitor (ML 9811, Monitor Labs). HONO was measured by the sensitive LOPAP instrument (Long Path Absorption Photometer) which is explained in detail elsewhere [47,48]. For experiments with pure HONO a commercial HONO source was used (QUMA) the working principle of which is explained elsewhere [49].

To investigate the formation of the inorganic reaction products nitrite (NO_2^-) and nitrate (NO_3^-) on the surface of the material, the coated glass plate was extracted in 100 mL ultra-pure water for 1 h subsequently after an experimental run. The extract was filtered using a 0.45 µm polyethersulfone syringe filter (Wicom) and finally analyzed by ion chromatography (Compact IC 761, Metrohm). The separation was carried out isocraticly on a Metrosep A Supp 5 – 250/4.0 column using a mixture of $NaHCO_3$ (1.0 mM) and Na_2CO_3 (3.2 mM) and a flow rate of 0.7 mL min^{-1}. The limit of detection was 0.05 mg L^{-1} NO_2^- and 0.04 mg L^{-1} NO_3^-.

The errors given later in Section 3 always represent the 1 σ standard deviation for n measurements.

2.4. Kinetic parameters

The experimental set-up in this study enables the determination of first order rate constants k_{rxn} (s^{-1}), following the decay of the reactants as a function of time, according to:

$$k_{rxn} = -\frac{\ln\left(c_t/c_0\right)}{t_{rxn}} \quad \text{(E-I)}$$

with the reactant concentration at the inlet c_0 and the outlet c_t and t_{rxn} (s) as reaction time. To be independent on the geometry of the reactor, uptake coefficients $\gamma_{geom.}$ are further calculated according to:

$$\gamma_{geom.} = \frac{4 \cdot k_{rxn}}{\bar{v} \cdot \left(S_{active}/V\right)} \quad \text{(E-II)}$$

with the geometric surface area S_{active} (m^2), the reactor volume V above the sample (m^3) and the molecular velocity of the reactant $\bar{v}$ (m s^{-1}) given by the gas-kinetic theory:

$$\bar{v} = \sqrt{\frac{8 \cdot R \cdot T}{\pi \cdot M}} \quad \text{(E-III)}$$

for which R, T and M represent the ideal gas constant (8.314 J mol^{-1} K^{-1}), the absolute temperature T (K) and the molecular mass of the reactant M (kg mol^{-1}), respectively. To avoid uncertainties by determining the reactor volume and t_{rxn}, due to the rough sample surface, $\gamma_{geom.}$ was finally calculated using the gas flow rate ϕ_{gas} (m^3 s^{-1}):

$$\gamma_{geom.} = -\frac{4 \cdot \ln\left(c_t/c_0\right) \cdot \phi_{gas}}{\bar{v} \cdot (S_{active})} \quad \text{(E-IV)}$$

It should be noted here that $\gamma_{geom.}$ will be derived for different measuring periods with Light OFF and Light ON, where Light ON means the sum of dark and light influence and is therefore always indexed by (Light ON = total).

To calculate deposition fluxes in atmospheric models the surface resistance (R_c) is calculated from the inverse of the surface deposition velocity v_{surf} (m s^{-1}):

$$v_{surf} = \frac{\gamma_{geom.} \cdot \bar{v}}{4} \quad \text{(E-V)}$$

Detailed information on the reaction kinetic parameters are given elsewhere [50].

3. Results and discussion

The impact of a photocatalytically active cement-based material on NO_x to improve urban air quality is assessed, first by plugged flow photoreactor experiments with pure NO, NO_2 and HONO in Section 3.1. Then, the influence of the experimental conditions on the photocatalytic performance is discussed in Section 3.2. Finally the formation of reaction products in the aqueous extract of the active surface and potentially in the gas phase is evaluated in Section 3.3.

3.1. Photocatalytic experiments with NO, NO_2 and HONO

Sample plates coated with both materials (A or B), have been investigated and always compared to the inactive reference material (R_i). The obtained results in the following subsections are typically explained using material A and R_i as example. However, the derived uptake coefficients for all tested materials are summarized in Table 1.

3.1.1. NO

The results of the photoreactor experiments with 100 ppb NO and material A compared to the inactive reference are shown in Fig. 2.

Both experiments started by adjusting the starting mixing ratio of

Table 1
$\gamma_{geom.}$ Light OFF and Light ON for the experiments with NO, NO_2 and HONO using the active materials A and B compared to the inactive reference material R_i.

Air pollutant	Material	$\gamma_{geom.}$ (Light OFF)	$\gamma_{geom.}$ (Light ON = total)
NO	A	$< 5 \times 10^{-7}$	$(5.1 \pm 0.7) \times 10^{-5}$
	B	$(9 \pm 5) \times 10^{-7}$	$(5.7 \pm 0.8) \times 10^{-5}$
	R_i	$< 5 \times 10^{-7}$	$< 5 \times 10^{-7}$
	A - R_i	$< 5 \times 10^{-7}$	$(5.1 \pm 0.7) \times 10^{-5}$
	B - R_i	$(9 \pm 5) \times 10^{-7}$	$(5.7 \pm 0.8) \times 10^{-5}$
NO_2	A	$(4.3 \pm 0.6) \times 10^{-6}$	$(4.7 \pm 0.7) \times 10^{-5}$
	B	$(8.4 \pm 1.2) \times 10^{-6}$	$(6.0 \pm 0.8) \times 10^{-5}$
	R_i	$(3.1 \pm 0.5) \times 10^{-6}$	$(4.1 \pm 0.6) \times 10^{-6}$
	A - R_i	$(1.2 \pm 1.0) \times 10^{-6}$	$(4.3 \pm 0.8) \times 10^{-5}$
	B - R_i	$(5.3 \pm 1.6) \times 10^{-6}$	$(5.6 \pm 0.9) \times 10^{-5}$
HONO	A	$(7.1 \pm 1.1) \times 10^{-5}$	$(7.0 \pm 1.1) \times 10^{-5}$
	B	Not measured	Not measured
	R_i	$(7.1 \pm 1.1) \times 10^{-5}$	$(6.8 \pm 1.1) \times 10^{-5}$
	A - R_i	$< 2 \times 10^{-6}$	$< 2 \times 10^{-6}$
	B - R_i	Not measured	Not measured

100 ± 2 ppb NO during the bypassing period. The injection of this gas phase flow into the reactor under dark conditions did not led, for both materials, to any sustained loss of NO, indicating that only adsorption with no further dark reaction of NO at the surface is taking place, in agreement with studies on pure TiO_2 [51–53]. However, the active and reference samples did shown contrasting behaviors when the lamps were switched on. Whereas almost no difference is observed using material R_i, the values for NO decreased significantly to below 20 ppb while NO_2 increased up to 10 ppb. Finally, NO and NO_2 values reached about 10 ppb in Fig. 2a) under steady state conditions, clearly emphasizing the photocatalytic ability of material A to remove NO from the gas phase. These steady state values were used to derive the uptake coefficient $\gamma_{geom.}$(NO) during Light ON in Fig. 2a) that is $(5.1 \pm 0.7) \times 10^{-5}$ and $< 5.0 \times 10^{-7}$ for material R_i in Fig. 2b). For comparison $\gamma_{geom.}$(Light OFF) is more than two orders of magnitude smaller (see Table 1) demonstrating the photocatalytic activity, that is mostly explained in the literature by the following reactions (R-2)-(R-11) resulting in nitrate as final reaction product at the surface [42,51,54].

$$h^+_{VB} + H_2O_{(ads)} \rightarrow {}^{\bullet}OH_{(ads)} + H^+ \quad \text{(R-2)}$$

$$e^-_{CB} + O_{2(ads)} \rightarrow O^{\bullet-}_{2(ads)} \quad \text{(R-3)}$$

$$O^{\bullet-}_{2(ads)} + H^+ \rightarrow HO^{\bullet}_{2(ads)} \quad \text{(R-4)}$$

$$NO_{(ads)} + {}^{\bullet}OH_{(ads)} \rightarrow HONO_{(ads)} \quad \text{(R-5)}$$

$$NO_{(ads)} + HO^{\bullet}_{2(ads)} \rightarrow NO_{2(ads)} + {}^{\bullet}OH_{(ads)} \quad \text{(R-6)}$$

$$NO_{2(ads)} + e^-_{CB} \rightarrow NO^-_{2(ads)} \quad \text{(R-7)}$$

$$NO_{2(ads)} + O^{\bullet-}_{2(ads)} \rightarrow NO^-_{2(ads)} + O_2 \quad \text{(R-8)}$$

$$NO^-_{2(ads)} + H^+ \rightleftarrows HONO_{(ads)} \quad \text{(R-9)}$$

$$NO^-_{2(ads)} + 2{}^{\bullet}OH \rightarrow NO^-_{3(ads)} + H_2O \quad \text{(R-10)}$$

$$NO_{2(ads)} + {}^{\bullet}OH_{(ads)} \rightarrow HNO_{3(ads)} \rightleftarrows NO^-_{3(ads)} + H^+ \quad \text{(R-11)}$$

The production of NO_2 during Light ON using material A in Fig. 2a) clearly indicates that NO_2 is an intermediate reaction product during the photocatalytic NO-oxidation as given by reaction (R-6). Since NO_2 is the air quality controlled pollutant, this process has to be considered. However, it has to be noted here, that the molybdenum based NO_x-analyzer is subject to interferences and therefore not really specific to NO_2. Therefore, an interference of so called NO_y-reaction products, like HONO, cannot be excluded [50]. However, direct HONO measurements using the LOPAP instrument demonstrated no significant photocatalytic HONO production in the gas phase during the experiments with pure NO, minimizing the interference issue.

3.1.2. NO_2

Similar experiments were also performed using a gas flow containing 100 ppb NO_2, but here a decrease of the NO_2 concentration was already observed in the dark, with a slow passivation of the surface, see Fig. 3.

This is significantly different to the behavior observed for NO in Fig. 2 and demonstrates that NO_2 already interacts with the surface under dark conditions as a result, for example, of the reaction with water (50% RH) present at the surface [55], as given by reaction (R-12)

$$2NO_{2(ads)} + H_2O_{(ads)} \rightarrow HONO_{(ads)} + HNO_{3(ads)} \quad \text{(R-12)}$$

or after adsorption of NO_2 on TiO_2 surface by intra- and intermolecular disproportionation reaction of the formed N_2O_4 as discussed by Sivachandiran, et al. [56] for NO_2 on pure TiO_2. Due to this, $\gamma_{geom.}$(Light OFF) is 3–4 × 10^{-6} for both materials and has to be considered for further evaluation of the photocatalytic activity of the tested material. However, as can be seen by comparing Fig. 3a) and b) the results for the Light ON periods are significantly different. NO_2 decreased to values

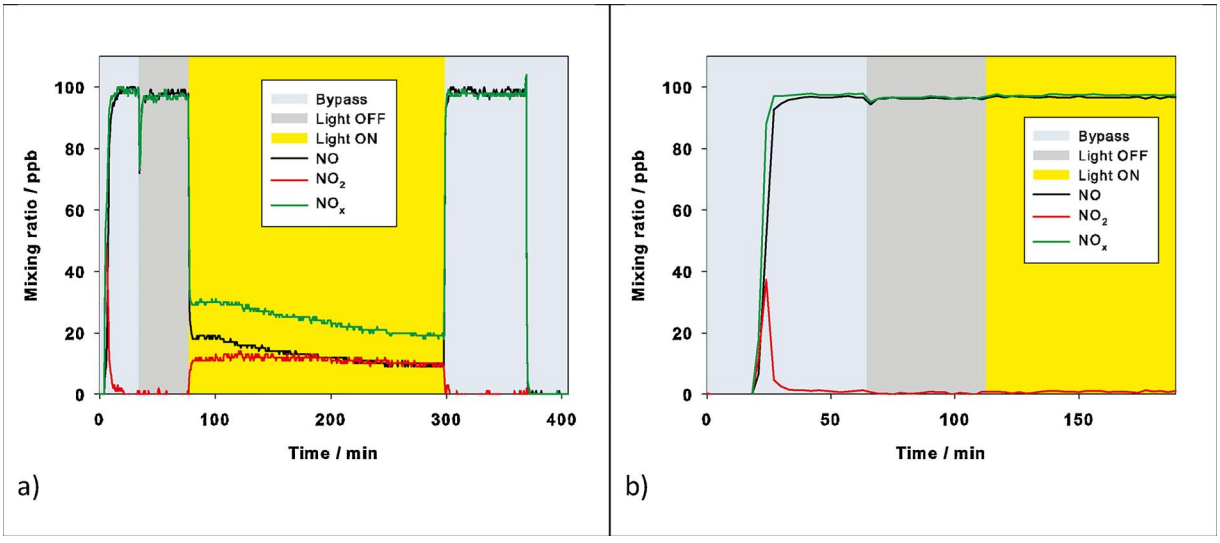

Fig. 2. NO, NO_2 and NO_x mixing ratios during the different measuring phases i.e., bypass, Light OFF and Light ON for the exp. conditions: 3 L min^{-1}, 50% RH, 21 W m^{-2} and 100 ppb NO with a) material A and b) material R_i.

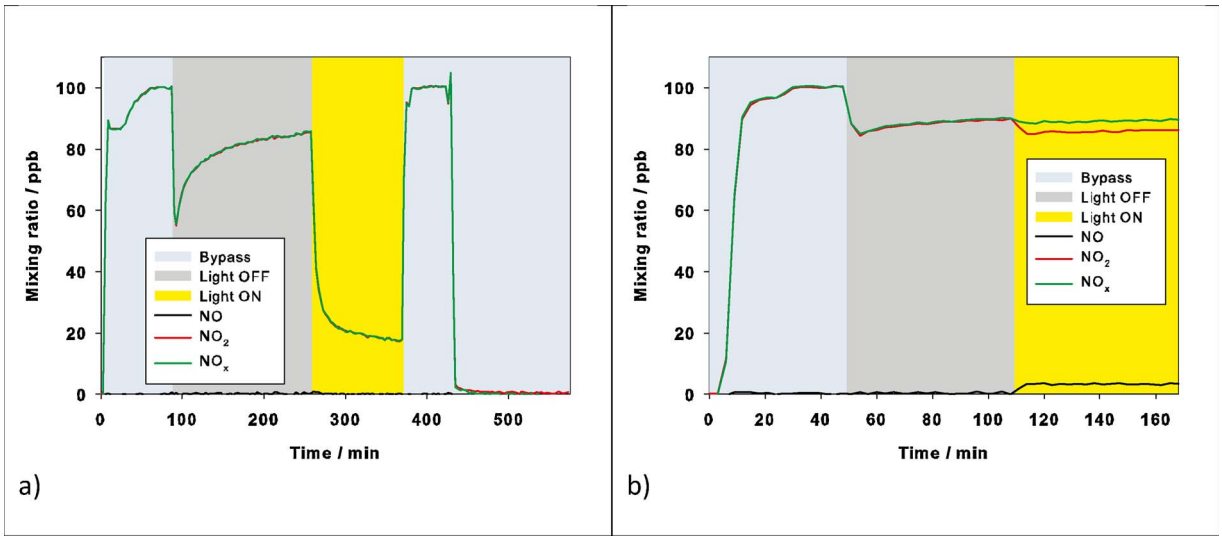

Fig. 3. NO, NO_2 and NO_x during the different measuring phases i.e., bypass, Light OFF and Light ON for the exp. conditions: 3 L min^{-1}, 50% RH, 21 W m^{-2} and 100 ppb NO_2 with a) material A and b) material R_i.

below 20 ppb using the active material A when the UV-light is switched on. But this effect is, in contrast to the results for NO, not directly and solely related to photocatalysis as presented by reaction (R-7)-(R-11). As shown in Fig. 3b) using material R_i, gas phase and adsorbed NO_2 is photolyzed under irradiation with UV-light ($\lambda < 424$ nm) resulting in the formation of NO (and subsequently O_3) which has to be taken into account for the assessment of $\gamma_{geom.}$Light ON using the active material A. Therefore, the real uptake coefficient is given by the difference of the active and the inactive material. The obtained $\gamma_{geom.}$(Light ON = total) of NO_2 is $(4.3 \pm 0.8) \times 10^{-5}$ for material A and thus in a similar range as measured for NO.

Similar to the experiments with NO only small HONO formation was observed, which was even smaller compared to the blank formation in the empty reactor resulting e.g., by reaction (R-12) on the Teflon and glass surfaces. This smaller HONO concentration in the presence of the cement-based samples indicate efficient uptake of HONO on the alkaline samples.

Since surface adsorbed oxygen is one reactant proposed to be involved in the photocatalytic oxidation of NO and NO_2 (see reaction (R-3), (R-4) and (R-8)) the carrier gas composition was varied to investigate the influence of oxygen on the photocatalytic reactivity of the cement-based material. Fig. 4 shows the results for NO and NO_2 using clean air (20% O_2) in comparison to pure nitrogen as carrier gas.

The results in Fig. 4a) demonstrate the significant impact of O_2 on the photocatalytic activity of material A to decompose NO. Whereas no difference is observed without light, a clear change in the shape of the NO-signal appears after switching on the UV-light. The values of NO decreased from 97 ppb to 12 ppb ($\gamma_{geom.}$ 4.6×10^{-5}) and remained constant under steady state conditions using clean air. Taking the formation of NO_2 into account, the overall difference for NO_x between Light OFF and Light ON is about 75 ppb. In contrast, the NO-values show only a small drop (probably due to residual O_2 adsorbed on the surface) and increase back to the values under dark conditions within 30 min with pure N_2 as carrier gas. The derived uptake coefficient in the absence of O_2 is therefore two orders of magnitude smaller ($< 5 \times 10^{-7}$) compared to clean air, demonstrating that the often proposed oxidation of NO with OH radicals (R-5) is only a very minor reaction path for the tested cement-based surfaces. Also the missing formation of NO_2 emphasizes an O_2 dependent photocatalytic NO-oxidation pathway for the tested material. Thus, the results in Fig. 4a) prove that the dominating initial step has to be the reaction of the conduction band electron with adsorbed O_2 (see reaction (R-3)), thereby preventing charge

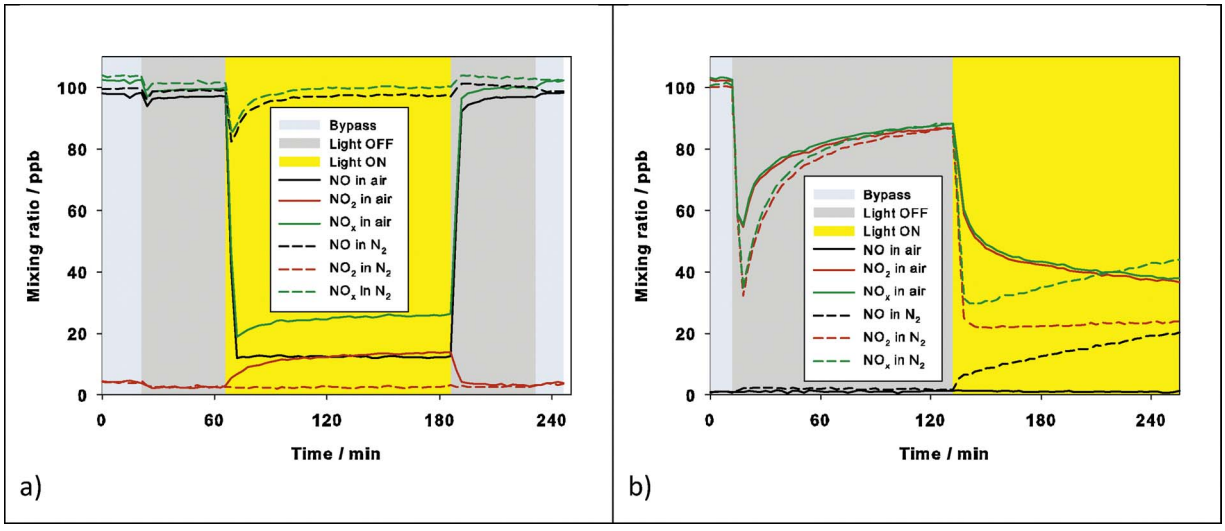

Fig. 4. Carrier gas dependence of the degradation of NO, NO_2 and NO_x on material A: clean air (solid lines) vs. nitrogen (N_2, dashed lines) for the measuring phases Bypass, Light OFF and Light ON. Exp. conditions: 3 L min^{-1}, 50% RH, 21 W m^{-2} a) 100 ppb NO and b) 100 ppb NO_2.

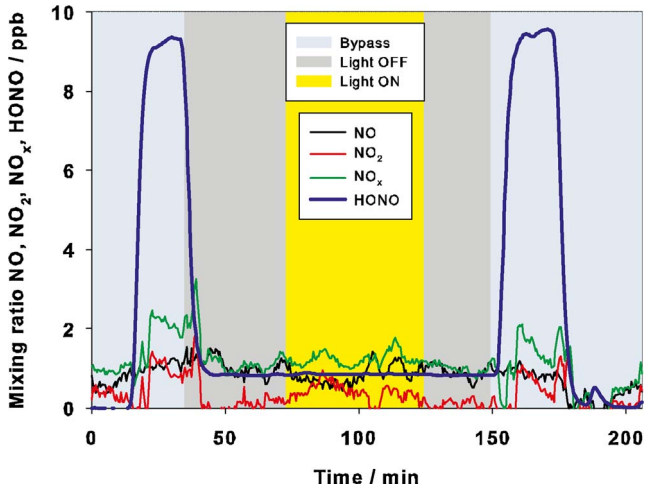

Fig. 5. HONO, NO, NO_2 and NO_x during the uptake of pure HONO on material A. Exp. conditions: 3 L min^{-1}, 40% RH, 15 W m^{-2} and ~10 ppb HONO.

recombination as previously observed in studies on other substrates, like pure TiO_2 [51], a photocatalytic paint [6] or TiO_2-coated mortars [11]. The formation of the hydroperoxyl radical (HO_2·) and the subsequent oxidation of NO as presented by reaction (R-4) and (R-6) is an often proposed mechanism on TiO_2-containing surfaces [6,42,52]. Due to the alkaline surface of the cement-based material (pH 10) and a pKs-value of 4.8 for HO_2 [57] the equilibrium given in (R-13) is fully on the left side.

$$O_2^{\bullet -} + H_2O \rightleftharpoons HO_2^{\bullet} + OH^- \quad \text{(R-13)}$$

Therefore, reactions (R-4)–(R-6) can be excluded for the experiments in this study. Instead, the oxidation of NO occurs probably directly by O_2^- via peroxynitrite as intermediate product (R-14) as suggested by former studies on pure TiO_2 [58,59] and TiO_2containing concrete [17].

$$NO_{(ads)} + O_{2(ads)}^{\bullet -} \rightarrow ONOO_{(ads)}^- \quad \text{(R-14)}$$

All studies on the photocatalysis of NO_x propose the formation of nitrate as the final reaction product. However, due to the alkaline surface in the present study a direct formation is excluded. The pKs for HOONO is 6–8 and results in 99% of the peroxynitrite anion at the surface that require further reactions to form the observed NO_2 intermediate and nitrate as the final reaction product. Internal conversion [60] or homolysis of HOONO and recombination in the solvent cage [61] can be neglected due to the alkaline surface properties. Possible pathways, however are reactions (R-15) and (R-16) based on laboratory studies of aqueous phase radical chemistry [62,63] in agreement with the experimental results in the present study.

$$^{\bullet}OH_{(ads)} + ONOO_{(ads)}^- \rightarrow H^+ + O_{2(ads)}^{\bullet -} + NO_{2(ads)}^- \quad \text{(R-15)}$$

$$NO_{(ads)} + ONOO_{(ads)}^- \rightarrow NO_{2(ads)} + NO_{2(ads)}^- \quad \text{(R-16)}$$

Adsorbed nitrite can further react either with a hole (h_{vb}^+) or other hydroxyl radicals (OH) (R-10) to form the observed final product nitrate.

Although the shape of the time dependent NO_2 uptake curve on the surface in the dark is slightly different for clean air and pure nitrogen, the final steady state uptake is similar for both buffer gases. The stronger initial uptake of NO_2 in the dark in N_2 indicates a stronger competition of O_2 with NO_2 compared to N_2 for adsorption on free active sites at the surface and influences consequently also the difference during the Light ON period shown in Fig. 4b). The competition of O_2 and NO_2 for the conduction band electrons is obviously an important process step for the photocatalytic activity of the tested material, indicated by the slower decrease of NO_2 and the much later achievement of the steady state conditions using clean air compared to pure nitrogen. The derived uptake coefficient during Light ON therefore is a factor 1.5 higher for N_2 than for clean air. A renoxification process of the reaction product nitrate at the surface [44] explains the increasing formation of NO as observed during irradiation using nitrogen as carrier gas in Fig. 4b. In addition, because of the necessity of O_2 for the photocatalytic decomposition of NO, the continuously increasing NO level only in N_2 is explained by the increasing nitrate on the surface by (R-11) and its consecutive renoxification. In contrast, when using pure air a much faster photocatalytic oxidation of NO (R-6) compared to a slower renoxification, suppress its formation. The photolysis of the sometimes proposed intermediate product HONO [39,41,64] can be neglected as NO-source, because the alkaline surface of the used material (pKs_{HONO} = 3.29) shifts the equilibrium (R-9) to the more stable nitrite. In addition the potential HONO-source reaction (R-5) was excluded above by the experiments with NO in N_2. With that, it becomes clear that the dominating initial step of the photocatalytic NO_2-decomposition is the reaction with the hydroxyl radical (R-11) which is independent on O_2 (see above and [6]). According to this reaction nitrate is expected as final photocatalytic reaction product. This is further discussed in Section 3.3.

3.1.3. HONO

The uptake of HONO was studied using a pure HONO source [49] on material A. The results in Fig. 5 clearly demonstrate a significant uptake of HONO on the investigated sample already in the dark with $\gamma_{geom.}$(Light OFF) 7.0×10^{-5}. This behavior can be explained by the very alkaline surface properties of the cement-based material, for which the equilibrium HONO⇌NO_2^- (R-9) is shifted to the highly soluble nitrite. However, as can be seen for Light ON in Fig. 5, no additional HONO reduction was observed under irradiation resulting in $\gamma_{geom.}$ (Light ON = total) again 7.0×10^{-5}. In conclusion, there is no measurable photocatalytic activity of the tested material A for HONO under the used simulated atmospheric conditions (see Table 1). The missing formation of NO_2 during UV irradiation (see Fig. 5) also confirms that an oxidation of HONO/NO_2^- to NO_2 as an intermediate step during oxidation to the final product nitrate (see (R-10)), as often proposed in many other studies, is of minor importance and not further considered in the mechanism ((R-1)–(R-11)). presented above. This reaction was also excluded in another study [6], in which the photocatalysis of HONO was explicitly studied, in contrast to most former studies which proposed NO_2 intermediate formation from HONO oxidation.

For a comprehensive overview, the derived uptake coefficients for NO, NO_2 and HONO using material A, B and R_i are summarized in Table 1.

As can be seen from Table 1, material B with the higher amount of the photocatalyst TiO_2 shows also slightly higher uptake coefficients for NO and NO_2, although the differences are near the accuracy errors of the measurements. Thus, the present plugged flow photoreactor experiments in summary of Section 3.1 have proven the ability of the tested cement-based materials A and B to depollute air contaminated with NO and NO_2 ($\gamma_{geom.}$(Light ON = total) = ~5×10^{-5}). In contrast no photocatalytic degradation was observed for HONO. The alkaline surface properties of the cement samples can already efficiently trap this harmful pollutant with an uptake coefficient $\gamma_{geom.}$ = ~7×10^{-5}. Depending on the surface acidity and with respect of the pH-dependent equilibrium (R-9), HONO can either be trapped as nitrite (present study) or released as HONO to the gas phase on acidic or neutral surfaces (e.g., Langridge, et al. [39]).

It should be highlighted that the activity of material A for its photocatalytic reaction was slightly but continuously increasing over the course of the extensive use (number of experimental runs including the cleaning procedure during the three years lab measurements). Thus, some of the data shown in the different plots of the present study are not directly comparable and reflect the changing activity of material A. In contrast, material B was much less used and showed the expected

higher activity (with respect to its higher TiO_2 content) only compared to freshly prepared material A, while to the end of the study both materials (A fully activated, B much less used) showed similar reactivity (see Table 1).

The differences between the freshly prepared material A and the "fully activated" are explained by side reactions of photocatalytically formed OH radicals (R-2) with organic additives in the cement-based material. The tested material (A, B and R_i) contained about 1.0 ± 0.3% of organic carbon. Details on the measuring procedure are given in SI 1. The photocatalytic self-degradation process of organics in the coating was proven by experiments with material B with and without the additive and in comparison with material R_i (see SI 4–6). The emission of formaldehyde is only observed if the organic additive and the photocatalyst TiO_2 are present at the irradiated surface. The formation of C1-C5 aldehydes was also confirmed in chamber studies by Mothes, et al. [44]. Long-term experiments were not directly performed in the present study. However, when all hours of irradiation are summed up the emission of formaldehyde decreases with time but is still present after more than 500 h (cf. SI 7). Since HO_2/O_2^--radicals show much lower reactivity against organics compared to the OH-radical [65–72] the organics at the surface were mainly in competition with the air pollutants for the OH-radicals. For freshly prepared surfaces the OH radicals reacted with the organic additive, leading to a lower activity. When the amount of additives at the surface was decreasing in response of the photocatalytic side reaction (see decreasing aldehyde formation), the activity increased caused by the increasing levels of free active surface sites and surviving OH-radicals.

These results have several important consequences. First, photocatalytic materials including binders and additives should be optimized for high stability against the photocatalytic oxidation to minimize undesired formation of harmful aldehydes from the coating alone, as observed also in other studies (e.g., Auvinen and Wirtanen [8]). Second, before testing photocatalytic surfaces for their activity, they should be activated by UV-irradiation as long as those undesired side reactions diminish. However, for the material used in the present study significant activation time of the order of at least several weeks of full irradiation is necessary. Thus other additives leading to less aldehyde formation might be used in the future. And finally, the use of only NO in standard tests of the photocatalytic activity (see e.g., ISO 22197-1) is not recommended. Since NO is the only main trace gas which is oxidized by HO_2/O_2^-radicals, while other main pollutants (e.g., VOCs, NO_2, HONO,…) are oxidized by OH-radicals on photocatalytic surfaces, the use of NO_2 is highly recommended here (for details see also Ifang, et al. [50]). NO_2 is not only a more important urban pollutant, but its activity is also a much better measure for the general activity of photocatalytic surfaces against main urban pollutants.

3.2. Impact of experimental conditions on the photocatalytic effect

To assess the impact of the photocatalytically active material on urban air quality, it is necessary to characterize in detail the influence of the variable ambient conditions. Therefore, the relative humidity, flow rate, starting mixing ratio and light intensity have been varied. The results are again discussed for material A. Only in the event of different results obtained for material B it is highlighted and discussed in the respective subsection.

3.2.1. Dependence on RH

The impact of RH on the photocatalytic activity of pure TiO_2 or embedded in different substrates applied to NO_x abatement is under controversial discussion in the scientific community [11,73]. The effect is based on two contrary contributions of water. H_2O can interact with the active surface either increasing the reactivity due to the formation of reactive radicals (see reactions (R-2) and (R-4)) or lowering the activity by blocking the adsorption of the target compounds to the active sites [31].

In this study, the derived uptake coefficients $\gamma_{geom.}(NO)$ and $\gamma_{geom.}(NO_2)$ for Light ON decreased from 6.0×10^{-5} to 1.1×10^{-5} with increasing humidity as given in SI 8. However, the results imply two separated sections. Under consideration of the 1 σ standard deviation $\gamma_{geom.}$ NO and NO_2 are in a similar range for RH between 0 and 25%, whereas further increase of RH up to 87% results in a constant decrease of the uptake coefficients. When extrapolating these curves to 100% RH no significant photocatalytic activity is expected for a multilayer water surface layer. These findings confirm the two contrary contributions of H_2O to the photocatalytic performance of the tested material. The observed dependence on RH indicates that the competition for the active surface sites is the dominating and therefore limiting process for typical atmospheric humidities (> 25% RH).

For pure nitrous acid (HONO) no significant variation of the uptake kinetics with humidity (20%–85% RH) was observed, which is explained by the simple physical adsorption of HONO in the form of nitrite on the highly alkaline cement-based surface as mentioned before.

3.2.2. Dependence on gas flow rate

To prove that the determination of the uptake coefficients for this photoreactor study is valid and appropriate for the assessment of the photocatalytic effect under real atmospheric conditions, the flow rate was varied in the range of 2–7 L min^{-1} whereas all other parameters were kept constant. The derived uptake coefficients for NO and NO_2 during Light ON given in SI 9 showed no dependence on this experimental parameter, as expected for the flow rate independent uptake coefficients, confirming 1st order kinetic (see Section 2.4) in contrast to, e.g., degradation rates often used in the literature to quantify the photocatalytic degradation of NO_x. Thus, uptake coefficients – as recommended by IUPAC – should be used in the future for better comparison of experimental results in different reactors under different experimental conditions (flow rate, mixing ratio, S_{active}/V, etc.).

However, flat bed photoreactor experiments may be subject to transport limitations due to the supposed laminar flow behavior of the gas. Diffusion limitation as the result would lead to an underestimation of the real photocatalytic activity. However, caused by the independence of the uptake coefficient on the flow rate no significant diffusion limitation is expected [6]. In addition, experiments using turbulence barriers along the reaction chamber according to Ifang, et al. [50] were performed to exclude that issue for the ISO 22197-1 [46] requested flow rate of 3 L min^{-1}. In contrast to the study by Ifang, et al. [50], the results demonstrated that a transport limitation for the photoreactor experiments in the present study can be excluded (data not shown). Possible reasons are a higher flow rate and the high roughness of the cement-based sample surface both inducing turbulences for the applied flow rate of 3 L min^{-1} in contrast to the very flat paint samples and the lower gas flow rate used in Ifang, et al. [50].

3.2.3. Dependence on the initial mixing ratio

The initial mixing ratio of NO and NO_2 was varied in a range of 50–900 ppb, whereas the other experimental conditions were kept constant. As expected, the derived uptake coefficients for NO and NO_2 given in SI 10 decreased clearly for material A with increasing the starting mixing ratio of the air pollutant. Taken the 1 σ standard deviations into account, $\gamma_{geom.}(NO)$ for material A can be considered as almost similar only up to 200 ppb. This means that the reaction order changes to < 1 and an evaluation by 1st order kinetic is not valid for the entire tested range of pollutant concentration. The results indicated also that the higher amount of the photocatalyst TiO_2 in material B change the active surface properties leading to higher photocatalytic activity compared to the results for material A (cf. Table 1). Nevertheless, also $\gamma_{geom.}(NO_2)$ using material B showed a slightly negative dependence on the mixing ratio. Although it was not tested in detail as for NO, due to the formerly observed similarity, a limit of about 200 ppb is also assumed to be valid for NO_2. That means, when testing photocatalytic materials only atmospheric relevant NO_x levels should

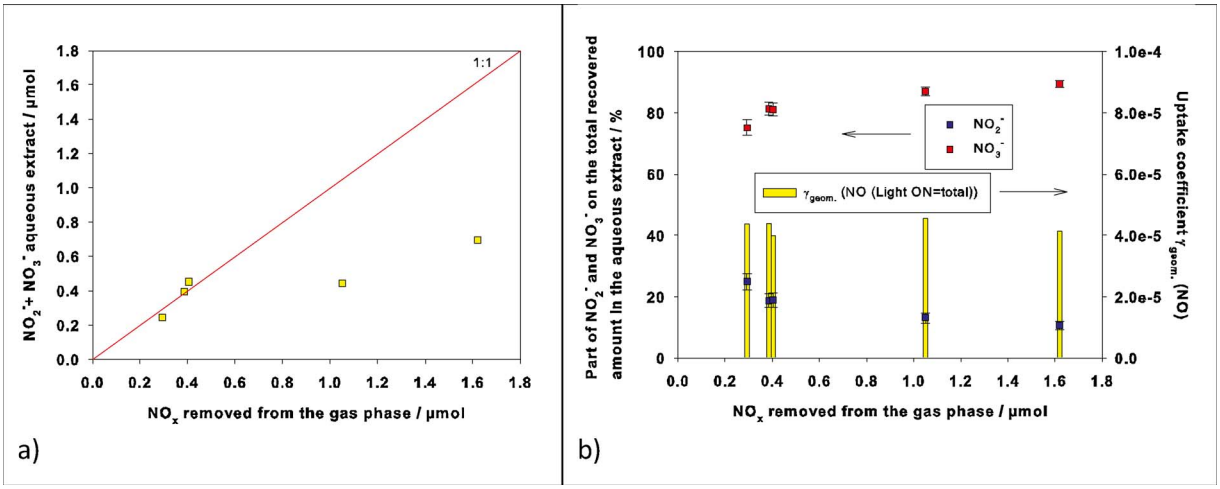

Fig. 6. NO_2^- and NO_3^- determined in the aqueous extract dependent on the amount of NO_x removed from the gas phase after the experiments with NO and material A: a) sum of NO_2^- and NO_3^- in µmol (the 1:1 line represents 100% recovery rate) and b) part of NO_2^- and NO_3^- in % of the total recovered amount in the aqueous extract (+ $\gamma_{geom.}$ (NO) Light ON). The amount of NO_x removed was varied by the duration of the experiment.

be applied under which first order kinetics are valid [50] not to underestimate the activity of the material, e.g., when using the ISO-norm recommended NO mixing ratio of 1 ppm.

Different theories exist to explain this change of the reaction order with air pollutant mixing ratio as observed in the present and previous studies on the photocatalytic performance of pure TiO_2 [51,74–76], mineral dust proxies [41], paints [6] or construction materials similar to the one in this study [11,14,33,50,54,77–81]. The most probable explanation based on the applied experimental conditions in the present study is the competition of the charge carrier recombination with diffusion to the surface followed by the photocatalytic reaction [82]. In contrast, a Langmuir-Hinshelwood-type mechanism, which is typically used to explain the saturation is more unlikely, since monolayer adsorption is typically observed at much higher reactant levels compared to those when zero order kinetics is observed in photocatalysis. This is also confirmed by the typical non-linear light intensity dependence of the photocatalytic degradation of NO_x (see SI 11).

In addition to NO and NO_2, the uptake of HONO was also studied for different starting mixing ratios in the range of 4–15 ppb on material A. In agreement with the results presented in Section 3.1 only strong dark uptake of HONO was observed on the alkaline surface of the cement-based material independent on the starting mixing ratio confirming 1st order kinetics (data not shown).

3.2.4. Dependence on light intensity

The measured dependence of the uptake coefficients for NO and NO_2 under variation of the light intensity in the range of 3–48 W m^{-2} (300–400 nm) clearly shows an increase of $\gamma_{geom.}$(NO) and (NO_2) with increasing the light intensity (see SI 11). However, this is only valid until approx. 20 W m^{-2} for the given experimental conditions. A higher light intensity do not result in a further increase of $\gamma_{geom.}$, but rather reach a maximum and finally staying constant until the highest tested value of 48 W m^{-2}. The observed non-linear response of the activity with light intensity is in agreement with other photocatalytic studies on NO and NO_2 using different types of materials [14,33,51,54,76,77,80,83–85]. Although the measured limit value for material A was approx. 20 W m^{-2} a light intensity of 21 W m^{-2} was often used due to technical issues in this study.

3.3. Product studies

Testing in detail the formation of reaction products is an essential part to assess the overall performance of the cement-based photocatalytically active material prior any real atmosphere application. Therefore, the formation of the expected final reaction products at the surface, in the aqueous extract of the surface, respectively and potentially in the gas phase has been examined.

3.3.1. Reaction products in the aqueous runoff and their dependence on the experimental conditions

The expected final reaction product of the photocatalytic NO_x-decomposition is the nitrate anion (NO_3^-) at the cement-based surface (see reactions (R-1)–(R-16)). The results of the ion chromatography analysis of the aqueous surface extract subsequently to experimental runs with NO as target pollutant are summarized in Fig. 6.

Nitrite (NO_2^-) and nitrate (NO_3^-) anions were identified as reaction products of the photocatalytic NO-decomposition using material A, as expected due to previous studies on pure TiO_2 [52,58,74,86] and other photocatalytically active construction materials [6,11,33–35]. Plotting the sum of NO_2^- and NO_3^- produced versus the consumption of gaseous NO_x (Fig. 6a)) enables the assessment of the recovery rate. The amount of NO_2 (constantly) formed during the Light ON period (cf. Fig. 2) is considered for the gaseous NO_x-consumption. As can be seen, an almost 100% recovery rate is observed for values up to 0.4 µmol NO_x, excluding further nitrogen containing reaction products. The distribution is about 20% NO_2^- and 80% NO_3^- (see Fig. 6b)). However, the amount of nitrate in studies using pure TiO_2 or photocatalytic paints is typically > 90%, whereas nitrite is only observed in traces [6,74]. Only one study [87] on the photocatalytic oxidation of NO_2 on TiO_2 showed, under high RH (80%), similar values for nitrite as in the present study. The measured 20% NO_2^- are therefore obviously related to the present material properties. Most likely, the pH 10 measured for the cement-based surface, which is in contrast to the studies on pure TiO_2 (pH 4–5 [74]) or paints (pH 8 [6]), promotes such formation of NO_2^- due to the thermodynamic stability of the oxidation states at the alkaline surface [34,35]. Furthermore, as can be seen in Fig. 6a), increasing the amount of NO_x removed from the gas phase results, despite constant uptake coefficients, in a clear deviation of the observed nitrite + nitrate values from the 1:1 line, indicating the formation of non-detected reaction products. However, extensive experimental tests on the extraction procedure (variation of the extraction time, application of different automatic shaking devices, etc.) proved its validity and excluded any negative influence of the extraction procedure on the decrease of the recovery rate. Therefore, the most probable reason is related to the influence of the material surface properties. Here, with increasing the reaction time it is likely that the reaction products can deeply enter the porous structure of the cement-based surface and interact with the current matrix that would explain the observed

deviation of the nitrite + nitrate values from the 1:1 line. The decreasing fraction of nitrite with the amount of NO_x removed (Fig. 6b)) is explained by the slow oxidation of the intermediate nitrite to nitrate by different oxidants with increasing reaction time, since the amount of NO_x removed was simply varied by the duration of the experiment. A further detailed investigation of the product formation mechanisms was, however, not in the focus of the present study. Moreover, for the application under real atmospheric conditions, it is more important to assess the impact of different applied conditions on the distribution of the reaction products at the surface.

Therefore for the reaction of NO_2, the influence of the most important experimental parameters RH and the starting mixing ratio (see Sections 3.2.2 and 3.2.4) on the product distribution was examined. The part of NO_2^- and NO_3^- on the total recovered amount in the aqueous extract in dependence of both parameters is shown in Fig. 7 (error bars represent an estimated uncertainty of 15%). The corresponding uptake coefficients for these experiments with NO_2 and material A are added on the respective right y-axes.

The results in Fig. 7a) show a clear dependence of the measured amounts of NO_2^- and NO_3^- on RH for a fixed starting mixing ratio of 100 ppb NO_2. The distribution was about 40/60% under dry conditions, changing to almost 100% NO_3^- at 50% RH and stayed constant when further increasing RH up to 88%. This behavior is explained similar to results obtained with a photocatalytic paint, for which also the oxidation of nitrite was increasing with humidity [6]. The formation of the intermediate nitrite is explained by reactions (R-7) and (R-8) which is further oxidized by the reaction with OH radicals (R-10) to nitrate. At low humidity nitrite will be present in the form of adsorbed HONO, while higher humidities will shift the equilibrium (R-9) to nitrite. Since only nitrite is efficiently oxidized by photocatalysis [9] the fraction of the intermediate nitrite will decrease with increasing humidity. In addition, increasing humidity may result in a higher quantity of available hydroxyl radicals promoting the photocatalytic oxidation of NO_2 and NO_2^-, respectively, to NO_3^- as the final reaction product, given by reactions (R-2), (R-10) and (R-11).

Fig. 7b) shows that also the starting mixing ratio of the target pollutant had an influence on the product distribution. Whereas for NO_2 < 100 ppb almost 100% NO_3^- were detected, the part of NO_2^- on the total recovered amount in the aqueous extract increases up to 10% for starting mixing ratios of about 900 ppb NO_2. This is again due to the previously discussed competition of NO_2 and water molecules for the active sites. Thus, at higher NO_2 mixing ratios the available OH radicals are all consumed by the NO_2, resulting in the observed higher amounts of nitrite that cannot be further oxidized by OH (R-10). In general, less available hydroxyl radicals result in a decrease of the complete photocatalytic NO_2-oxidation (see reaction (R-11)), in agreement with the overall observed dependence of $\gamma_{geom.}$ (NO_2) on the starting mixing ratio.

3.3.2. Extraction after the HONO experiments with material B

For the dark uptake of pure HONO only NO_2^- was observed confirming a simple physical adsorption. In contrast, when the photocatalytic uptake of HONO was studied under UV irradiation a near 100% NO_3^- yield demonstrates the secondary oxidation of NO_2^- by reaction (R-10) on material B. This confirms again that a direct photocatalytic oxidation of HONO can be excluded as the rate limiting step, see Section 3.1 and Fig. 5. The observed photocatalytic oxidation only of NO_2^- and not of HONO is in excellent agreement with a study on photocatalytic paints [6].

These results demonstrate the necessity to characterize the formation and distribution of reaction products in dependence on the material and the conditions of the planned application. A deactivation of the materials photocatalytic activity due to extensive product accumulation was never observed for the tested experimental conditions. However, the impact of accumulated reaction products on the formation of further products that can be released back to the gas phase will be discussed in the following Section 3.3.3.

3.3.3. Gas phase reaction products

For the photocatalytic reaction of NO, only NO_2 and non-significant traces of HONO were detected in the gas phase (see Section 3.1). Since NO_2 is an intermediate in the consecutive conversion NO → NO_2 → nitrate and since the further oxidation of NO_2 was found to be quite efficient ($\gamma \approx 5 \times 10^{-5}$) the intermediate formation of NO_2 is not a significant issue against the application of the used cement-based surfaces in the atmosphere. Besides this, NO_2 is the main NO_x species in a typical European urban daytime atmosphere further highlighting the need for efficient photocatalytic conversion of NO_2. This should be also considered in standard tests procedures of photocatalysis, for which up to now mainly the less important NO is considered, e.g. in ISO 22197-1.

For the other two investigated gas phase reactants NO_2 and HONO, no significant yields of gas phase products were observed.

However, gas phase renoxification through photocatalytic reaction of surface NO_3^- and subsequently formation of O_3 was recently proposed for photocatalytic active surfaces in chamber studies [43,44]. Thus, studies on this possible renoxification process were another focus of the present laboratory photoreactor experiments using the cement-based materials A and B.

Therefore, O_3 was measured in parallel to the photocatalytic NO_x-experiments. Fig. 8 shows the results for an experiment with 100 ppb NO_2 and material A.

In addition to the confirmation of the results presented in Section

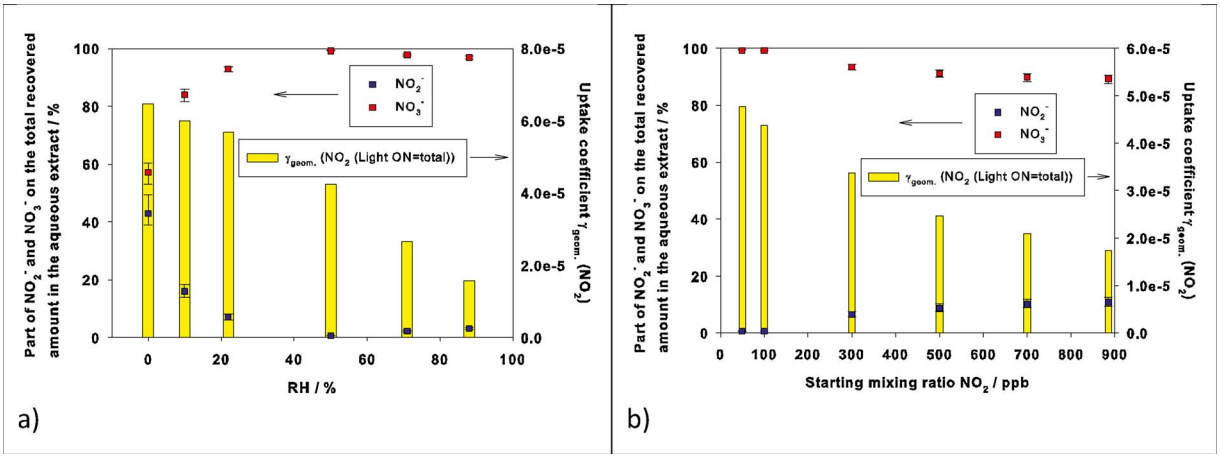

Fig. 7. NO_2^- and NO_3^- determined in the aqueous extract after the experiments with NO_2 and material A (+ $\gamma_{geom.}$ (NO_2) Light ON) dependent on a) RH with 100 ppb NO_2 and b) the starting mixing ratio for 50% RH.

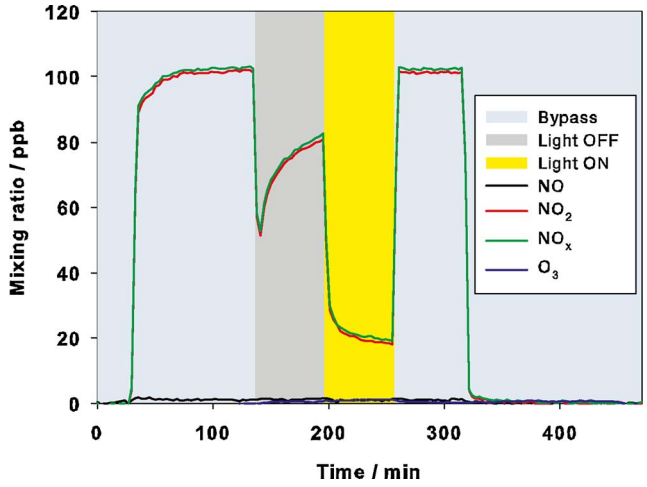

Fig. 8. NO, NO_2, NO_x and O_3 dependent on the measuring phases Bypass, Light OFF and Light ON and material A. Exp. conditions: 100 ppb NO_2, 3 L min^{-1}, 50% RH, 21 W m^{-2}.

3.1 the measured O_3 values are ≤ 1 ppb during all measuring periods as shown in Fig. 8. Thus, the photoreactor experiments with NO_2 following the experimental conditions of the ISO 22197-1 [46] do not indicate any significant renoxification process leading to a formation of O_3. This is, at least in part, explained by the typical short duration of the experiments leading only to small amounts of adsorbed nitrate.

Nevertheless, despite these experimental results, the observed O_3-formation using an almost identical cement-based material in photocatalytic chamber experiments with NO_x in Mothes, et al. [44] indicates an obviously crucial impact of the applied experimental setup and procedure. In these static simulation chamber experiments reaction times of several hours were applied, while in the present flow experiments the reactants are in contact to the photocatalytic surfaces for only approx. 1–2 s. Thus, any slow secondary O_3-formation may not be visible here.

Therefore, another test procedure using photoreactor experiments was applied to investigate a possible renoxification. For this purpose nitrate was added by an aqueous solution directly to the photocatalytically active surface and was dried by flushing with clean air. When the surfaces exposed to high levels of nitrate (approx. 1 g m^{-2}) were irradiated at high UV–light intensities (approx. 55 W m^{-2}) only a small formation of 2 ppb NO_2 and 0.5 ppb HONO, but no O_3 (< 1 ppb detection limit) were observed on the cement-based surface of material A. However, both species NO_2 and HONO are expected as byproducts of O_3 from the photocatalysis of nitrate and thus confirm a renoxification process for the tested complex photocatalytic material. That means, still more experiments are necessary to investigate for which experimental conditions and surface nitrate loadings the renoxification is an important atmospheric issue during typical rain wash-off periods and for typical atmospheric NO_x doses. In addition, possible high uptake of O_3 on the cement-based coating which might explain the missing O_3 formation during renoxification should be confirmed in the future.

In conclusion, the performed laboratory photoreactor experiments on the used cement-based material showed no additional atmospheric relevant formation of undesired gas phase reaction products like O_3 and HONO under the simulated atmospheric conditions. The low HONO yields are explained by the highly alkaline surface properties.

3.4. Remediation potential under realistic atmospheric urban condition

In the following section, upper limit photocatalytic NO_x-degradation is estimated in a typical urban main street canyon situation based on the laboratory results of the present study. Here, a street canyon with a cross section of 20 m × 20 m with the wind direction parallel to the canyon is considered (plugged flow situation). Next, it is assumed that the average wind speed (WS) in the canyon is WS = 1 m s^{-1} and that emitted NO_x will on average stay inside the canyon for 200 m until it escapes the canyon by vertical turbulent mixing, leading to an average NO_x reaction time of 200 s as an upper limit. For other wind directions, e.g. perpendicular to the canyon, higher turbulent mixing of the canyon air with the overlying atmosphere is expected, which would shorten the NO_x residence time in the canyon. To further maximize the degradation of pollutants, all the canyon surfaces (ground and walls) are assumed to be photocatalytically active with a surface reactivity similar to the present study. Total uptake coefficients under 20 W m^{-2} UV-A irradiation of 5×10^{-5} were thus used for both NO and NO_2, see Table 1. To calculate a first order rate coefficient inside the canyon, transport limitations have to be considered, for which typically resistance models including the turbulent mixing (resistance R_a), quasi molecular diffusion (R_b) and the surface activity (R_c) are considered (see e.g., VDI 3782, 2006 [88]) to calculate the uptake on surfaces in deposition models [50,89]. In the present study only the surface deposition velocity (1 / R_c) was used (E-V), see Section 2.4. To again calculate an upper limit remediation, transport limitations were neglected here (R_a, R_b = 0) and thus a well-mixed canyon situation and the absence of any concentration gradients towards the active surfaces were assumed. However, it should be stressed that the estimated NO_x uptake will be significantly overestimated by this simplification. Using e.g. the method described in VDI 3782 [88] to estimate R_a and R_b, the real uptake would decrease by 56% at a WS of 1 m s^{-1} and a surface deposition velocity of 0.5 cm s^{-1} by the transport limitation, i.e., more than a factor of two. On contrary, turbulences induced by moving vehicles (piston effect) may again decrease transport limitations.

Using the uptake coefficients of NO and NO_2 from the present study and a surface to volume ratio $S_{active}/V = 0.15\ m^{-1}$ of the canyon (see above), first order rate coefficients for NO and NO_2 degradation of $k(NO) = 8.6 \times 10^{-4}\ s^{-1}$ and $k(NO_2) = 7.0 \times 10^{-4}\ s^{-1}$ are calculated using Eqs. (E-I)–(E-IV), see Section 2.4. For simplicity we further used an average value $k(NO_x) = 7.8 \times 10^{-4}\ s^{-1}$. With the above specified upper limit reaction time of the air mass of t_{rxn} = 200 s and the identified first order reaction kinetics at atmospheric relevant concentrations (see Section 3.2.4), the NO_x-degradation is calculated by rearrangement of Eq. (E-I):

$$c_t/c_0 = e^{(-k_{NO_x} \cdot t_{rxn})} \quad \text{(E-VI)}$$

leading to a maximum estimated photocatalytic NO_x uptake of 14.4% at noontime conditions. Since the photocatalytic degradation will be zero during nighttime and assuming a) a 12 h day/night cycle and b) similar day- and nighttime NO_x-levels, half the average upper limit day and night NO_x remediation of ca. 7% is obtained. This value is more representative with respect to the active discussion about how to reach the annual average NO_2 threshold limit of 40 µg m^{-3} under urban conditions in Europe. However, it should be stressed that almost all variables were chosen here to obtain an upper limit remediation. For example, if reasonable transport limitations are considered according to VDI 3782 [88] and assuming only a 100 s mean NO_x residence time inside the canyon, an average reduction of only 1.7% is obtained. Here more detailed micrometeorological model studies including wind field, turbulence levels and transport limitations are required for the future. In addition, typically photocatalytic surfaces are not applied both, on the walls and on all ground surfaces as considered here, reducing the S_{active}/V ratio and accordingly the expected NO_x reduction. Furthermore, there are certain conditions under which photocatalytic surfaces will not work at all, e.g. on wetted surfaces (during/after rain events), in winter with snow and ice covered surfaces or when surfaces are exposed to salt solutions. In conclusion, an average NO_x remediation of only a few % is expected for a typical urban application of the studied photocatalytic surfaces, which is in good agreement with results from a recent model canyon study using similar surfaces in which an average NO_x reduction of approx. 2% was estimated [13].

As mentioned above, NO_x abatement, at the level of a few %, is achievable with efficient photocatalytic material. However, assessing its efficiency requires a few testing under specific conditions in order to be able to extrapolate to real atmospheric conditions. As highlighted by Ifang et al. [50], special attention has to be given to transport limitations and NO_2 gas phase photolysis in various type of reactors, leading to under- or over-estimations of activities, in addition to perform those tests under realistic atmospheric conditions. For instance, as NO_2 exhibit a much more relevant photochemistry, as compared to NO, those tests should involve this compound at atmospheric concentration (i.e., tens of ppb levels) and humidity (including higher RH). Under those circumstances, the impact of secondary processes can be investigated to ensure a proper assessment of the efficiency of the tested material. Only under such conditions are the uptake coefficients independent of the concentration level and the results can be extrapolated to any atmospheric conditions.

Acknowledgement

The authors gratefully acknowledge the financial support of the European Commission through the Life + grant LIFE 08 ENV/F/000487 PHOTOPAQ.

Appendix A. Supplementary data

Supplementary material related to this article can be found, in the online version, at doi: https://doi.org/10.1016/j.apcatb.2018.03.010.

References

[1] EEA Air Quality in Europe - 2016 Report No 28, (2016).
[2] C.B.B. Guerreiro, V. Foltescu, F. de Leeuw, Air quality status and trends in Europe, Atmos. Environ. 98 (2014) 376–384.
[3] J. Chen, C.-s. Poon, Photocatalytic construction and building materials: from fundamentals to applications, Build. Environ. 44 (2009) 1899–1906.
[4] S. Lacombe, F. Fresno, U.L. Štangar, Photocatalysis: new highlights from JEP 2013, Environ. Sci. Pollut. Res. 21 (2014) 11111–11115.
[5] A.H. Aïssa, E. Puzenat, A. Plassais, J.-M. Herrmann, C. Haehnel, C. Guillard, Characterization and photocatalytic performance in air of cementitious materials containing TiO_2. Case study of formaldehyde removal, Appl. Catal., B 107 (2011) 1–8.
[6] S. Laufs, G. Burgeth, W. Duttlinger, R. Kurtenbach, M. Maban, C. Thomas, P. Wiesen, J. Kleffmann, Conversion of nitrogen oxides on commercial photocatalytic dispersion paints, Atmos. Environ. 44 (2010) 2341–2349.
[7] J. Ângelo, L. Andrade, A. Mendes, Highly active photocatalytic paint for NO_x abatement under real-outdoor conditions, Appl. Catal., A 484 (2014) 17–25.
[8] J. Auvinen, L. Wirtanen, The influence of photocatalytic interior paints on indoor air quality, Atmos. Environ. 42 (2008) 4101–4112.
[9] A. Gandolfo, V. Bartolomei, E. Gomez-Alvarez, S. Tlili, S. Gligorovski, J. Kleffmann, H. Wortham, The effectiveness of indoor photocatalytic paints on NO_x and HONO levels, Appl. Catal., B 166–167 (2015) 84–90.
[10] T. Martinez, A. Bertron, G. Escadeillas, E. Ringot, V. Simon, BTEX abatement by photocatalytic TiO_2-bearing coatings applied to cement mortars, Build. Environ. 71 (2014) 186–192.
[11] T. Martinez, A. Bertron, E. Ringot, G. Escadeillas, Degradation of NO using photocatalytic coatings applied to different substrates, Build. Environ. 46 (2011) 1808–1816.
[12] M. Gallus, V. Akylas, F. Barmpas, A. Beeldens, E. Boonen, A. Boréave, M. Cazaunau, H. Chen, V. Daële, J.F. Doussin, Y. Dupart, C. Gaimoz, C. George, B. Grosselin, H. Herrmann, S. Ifang, R. Kurtenbach, M. Maille, A. Mellouki, K. Miet, F. Mothes, N. Moussiopoulos, L. Poulain, R. Rabe, P. Zapf, J. Kleffmann, Photocatalytic depollution in the Leopold II tunnel in Brussels: NO_x abatement results, Build. Environ. 84 (2015) 125–133.
[13] M. Gallus, R. Ciuraru, F. Mothes, V. Akylas, F. Barmpas, A. Beeldens, F. Bernard, E. Boonen, A. Boréave, M. Cazaunau, N. Charbonnel, H. Chen, V. Daële, Y. Dupart, C. Gaimoz, B. Grosselin, H. Herrmann, S. Ifang, R. Kurtenbach, M. Maille, I. Marjanovic, V. Michoud, A. Mellouki, K. Miet, N. Moussiopoulos, L. Poulain, P. Zapf, C. George, J.F. Doussin, J. Kleffmann, Photocatalytic abatement results from a model street canyon, Environ. Sci. Pollut. Res. 22 (2015) 18185–18196.
[14] J.K. Sikkema, S.K. Ong, J.E. Alleman, Photocatalytic concrete pavements: laboratory investigation of NO oxidation rate under varied environmental conditions, Constr. Build. Mater. 100 (2015) 305–314.
[15] C.H. Ao, S.C. Lee, C.L. Mak, L.Y. Chan, Photodegradation of volatile organic compounds (VOCs) and NO for indoor air purification using TiO_2: promotion versus inhibition effect of NO, Appl. Catal. B 42 (2003) 119–129.
[16] M.M. Ballari, M. Hunger, G. Hüsken, H.J.H. Brouwers, Modelling and experimental study of the NO_x photocatalytic degradation employing concrete pavement with titanium dioxide, Catal. Today 151 (2010) 71–76.
[17] M.M. Ballari, M. Hunger, G. Hüsken, H.J.H. Brouwers, NO_x photocatalytic degradation employing concrete pavement containing titanium dioxide, Appl. Catal. B 95 (2010) 245–254.
[18] C.L. Bianchi, S. Gatto, C. Pirola, A. Naldoni, A. Di Michele, G. Cerrato, V. Crocellà, V. Capucci, Photocatalytic degradation of acetone, acetaldehyde and toluene in gas-phase: comparison between nano and micro-sized TiO_2, Appl. Catal. B 146 (2014) 123–130.
[19] O. Debono, F. Thevenet, P. Gravejat, V. Hequet, C. Raillard, L. Lecoq, N. Locoge, Toluene photocatalytic oxidation at ppbv levels: kinetic investigation and carbon balance determination, Appl. Catal. B 106 (2011) 600–608.
[20] C. Mendoza, A. Valle, M. Castellote, A. Bahamonde, M. Faraldos, TiO_2 and TiO_2–SiO_2 coated cement: comparison of mechanic and photocatalytic properties, Appl. Catal. B 178 (2015) 155–164.
[21] C.C. Pei, W.W.F. Leung, Photocatalytic oxidation of nitrogen monoxide and o-xylene by TiO_2/ZnO/Bi_2O_3 nanofibers: optimization, kinetic modeling and mechanisms, Appl. Catal., B 174–175 (2015) 515–525.
[22] J.-M. Herrmann, Fundamentals and misconceptions in photocatalysis, J. Photochem. Photobiol. A Chem. 216 (2010) 85–93.
[23] M.R. Hoffmann, S.T. Martin, W. Choi, D.W. Bahnemann, Environmental applications of semiconductor photocatalysis, Chem. Rev. 95 (1995) 69–96.
[24] Y. Nosaka, A.Y. Nosaka, Generation and detection of reactive oxygen species in photocatalysis, Chem. Rev. 117 (2017) 11302–11336.
[25] J. Yi, C. Bahrini, C. Schoemaecker, C. Fittschen, W. Choi, Photocatalytic decomposition of H_2O_2 on different TiO_2 surfaces along with the concurrent generation of HO_2 radicals monitored using cavity ring down spectroscopy, J. Phys. Chem. C 116 (2012) 10090–10097.
[26] Y. Murakami, K. Endo, I. Ohta, A.Y. Nosaka, Y. Nosaka, Can OH radicals diffuse from the UV-irradiated photocatalytic TiO_2 surfaces? laser-induced-fluorescence study, J. Phys. Chem. C 111 (2007) 11339–11346.
[27] Y. Murakami, E. Kenji, A.Y. Nosaka, Y. Nosaka, Direct detection of OH radicals diffused to the gas phase from the UV-irradiated photocatalytic TiO_2 surfaces by means of laser-induced fluorescence spectroscopy, J. Phys. Chem. B 110 (2006) 16808–16811.
[28] J. Thiebaud, F. Thevenet, C. Fittschen, OH radicals and H_2O_2 molecules in the gas phase near to TiO_2 surfaces, J. Phys. Chem. C 114 (2010) 3082–3088.
[29] G. Vincent, A. Aluculesei, A. Parker, C. Fittschen, O. Zahraa, P.M. Marquaire, Direct detection of OH radicals and indirect detection of H2O2 molecules in the gas phase near a TiO_2 photocatalyst using LIF, J. Phys. Chem. C 112 (2008) 9115–9119.
[30] A.L. Linsebigler, G.Q. Lu, J.T. Yates, Photocatalysis on TiO_2 surfaces: principles, mechanisms, and selected results, Chem. Rev. 95 (1995) 735–758.
[31] H. Chen, C.E. Nanayakkara, V.H. Grassian, Titanium dioxide photocatalysis in atmospheric chemistry, Chem. Rev. 112 (2012) 5919–5948.
[32] R. de_Richter, S. Caillol, Fighting global warming: the potential of photocatalysis against CO_2, CH_4, N_2O, CFCs, tropospheric O_3, BC and other major contributors to climate change, J. Photochem. Photobiol. C 12 (2011) 1–19.
[33] N. Bengtsson, M. Castellote, Photocatalytic activity for NO degradation by construction materials: parametric study and multivariable correlations, J. Adv. Oxid. Technol. 13 (2010) 341–349.
[34] A. Folli, C. Pade, T.B. Hansen, T. De Marco, D.E. Macphee, TiO_2 photocatalysis in cementitious systems: insights into self-cleaning and depollution chemistry, Cem. Concr. Res. 42 (2012) 539–548.
[35] S. Karapati, T. Giannakopoulou, N. Todorova, N. Boukos, S. Antiohos, D. Papageorgiou, E. Chaniotakis, D. Dimotikali, C. Trapalis, TiO_2 functionalization for efficient NO_x removal in photoactive cement, Appl. Surf. Sci. 319 (2014) 29–36.
[36] K. Demeestere, J. Dewulf, H. Van Langenhove, Heterogeneous photocatalysis as an advanced oxidation process for the abatement of chlorinated, monocyclic aromatic and sulfurous volatile organic compounds in air: state of the art, Crit. Rev. Environ. Sci. Technol. 37 (2007) 489–538.
[37] J. Mo, Y. Zhang, Q. Xu, J.J. Lamson, R. Zhao, Photocatalytic purification of volatile organic compounds in indoor air: a literature review, Atmos. Environ. 43 (2009) 2229–2246.
[38] V. Bartolomei, M. Sörgel, S. Gligorovski, E.G. Alvarez, A. Gandolfo, R. Strekowski, E. Quivet, A. Held, C. Zetzsch, H. Wortham, Formation of indoor nitrous acid (HONO) by light-induced NO_2 heterogeneous reactions with white wall paint, Environ. Sci. Pollut. Res. 21 (2014) 9259–9269.
[39] J.M. Langridge, R.J. Gustafsson, P.T. Griffiths, R.A. Cox, R.M. Lambert, R.L. Jones, Solar driven nitrous acid formation on building material surfaces containing titanium dioxide: A concern for air quality in urban areas? Atmos. Environ. 43 (2009) 5128–5131.
[40] M. Ndour, P. Conchon, B. D'Anna, O. Ka, C. George, Photochemistry of mineral dust surface as a potential atmospheric renoxification process, Geophys. Res. Lett. 36 (2009) 1–4.
[41] M. Ndour, B. D'Anna, C. George, O. Ka, Y. Balkanski, J. Kleffmann, K. Stemmler, M. Ammann, Photoenhanced uptake of NO_2 on mineral dust: laboratory experiments and model simulations, Geophys. Res. Lett. 35 (2008) 1–5.
[42] M.E. Monge, B. D'Anna, C. George, Nitrogen dioxide removal and nitrous acid formation on titanium oxide surfaces—an air quality remediation process? Phys. Chem. Chem. Phys. 12 (2010) 8991–8998.
[43] M.E. Monge, C. George, B. D'Anna, J.-F. Doussin, A. Jammoul, J. Wang, G. Eyglunent, G. Solignac, V. Daële, A. Mellouki, Ozone formation from illuminated titanium dioxide surfaces, J. Am. Chem. Soc. 132 (2010) 8234–8235.
[44] F. Mothes, O. Böge, H. Herrmann, A chamber study on the reactions of O_3, NO, NO_2 and selected VOCs with a photocatalytically active cementitious coating material, Environ. Sci. Pollut. Res. 23 (2016) 15250–15261.

[45] E. Boonen, V. Akylas, F. Barmpas, A. Boréave, L. Bottalico, M. Cazaunau, H. Chen, V. Daële, T. De Marco, J.F. Doussin, C. Gaimoz, M. Gallus, C. George, N. Grand, B. Grosselin, G.L. Guerrini, H. Herrmann, S. Ifang, J. Kleffmann, R. Kurtenbach, M. Maille, G. Manganelli, A. Mellouki, K. Miet, F. Mothes, N. Moussiopoulos, L. Poulain, R. Rabe, P. Zapf, A. Beeldens, Construction of a photocatalytic de-polluting field site in the Leopold II tunnel in Brussels, J. Environ. Manage. 155 (2015) 136–144.
[46] ISO 22197-1, Fine Ceramics (Advanced Ceramics, Advanced Technical Ceramics) - Test Method for Air-Purification Performance of Semiconducting Photocatalytic Materials - Part 1: Removal of Nitric Oxide. Reference Number ISO 22197-1:2007(E), (2007) Switzerland.
[47] J. Heland, J. Kleffmann, R. Kurtenbach, P. Wiesen, A new instrument to measure gaseous nitrous acid (HONO) in the atmosphere, Environ. Sci. Technol. 35 (2001) 3207–3212.
[48] J. Kleffmann, J. Heland, R. Kurtenbach, J. Lörzer, P. Wiesen, A new instrument (LOPAP) for the detection of nitrous acid (HONO), Environ. Sci. Pollut. Res. (2002) 48–54.
[49] J. Kleffmann, T. Benter, P. Wiesen, Heterogeneous reaction of nitric acid with nitric oxide on glass surfaces under simulated atmospheric conditions, J. Phys. Chem. A 108 (2004) 5793–5799.
[50] S. Ifang, M. Gallus, S. Liedtke, R. Kurtenbach, P. Wiesen, J. Kleffmann, Standardization methods for testing photo-catalytic air remediation materials: problems and solution, Atmos. Environ. 91 (2014) 154–161.
[51] R. Dillert, A. Engel, J. Große, P. Lindner, D.W. Bahnemann, Light intensity dependence of the kinetics of the photocatalytic oxidation of nitrogen(II) oxide at the surface of TiO_2, Phys. Chem. Chem. Phys. 15 (2013) 20876–20886.
[52] Y. Ohko, Y. Nakamura, N. Negishi, S. Matsuzawa, K. Takeuchi, Photocatalytic oxidation of nitrogen monoxide using TiO_2 thin films under continuous UV light illumination, J. Photochem. Photobiol. A Chem. 205 (2009) 28–33.
[53] L. Sivachandiran, F. Thevenet, P. Gravejat, A. Rousseau, Investigation of NO and NO_2 adsorption mechanisms on TiO_2 at room temperature, Appl. Catal. B 142–143 (2013) 196–204.
[54] M.M. Ballari, Q.L. Yu, H.J.H. Brouwers, Experimental study of the NO and NO_2 degradation by photocatalytically active concrete, Catal. Today 161 (2011) 175–180.
[55] B.J. Finlayson-Pitts, L.M. Wingen, A.L. Sumner, D. Syomin, K.A. Ramazan, The heterogeneous hydrolysis of NO_2 in laboratory systems and in outdoor and indoor atmospheres: an integrated mechanism, Phys. Chem. Chem. Phys. 5 (2003) 223–242.
[56] L. Sivachandiran, F. Thevenet, A. Rousseau, D. Bianchi, NO_2 adsorption mechanism on TiO_2: an in-situ transmission infrared spectroscopy study, Appl. Catal. B 198 (2016) 411–419.
[57] B.H.J. Bielski, D.E. Cabelli, R.L. Arudi, A.B. Ross, Reactivity of HO_2/O_2^- radicals in aqueous solution, J. Phys. Chem. Ref. Data 14 (1985) 1041–1100.
[58] J.S. Dalton, P.A. Janes, N.G. Jones, J.A. Nicholson, K.R. Hallam, G.C. Allen, Photocatalytic oxidation of NO_x gases using TiO_2: a surface spectroscopic approach, Environ. Pollut. 120 (2002) 415–422.
[59] Z. Wu, Z. Sheng, H. Wang, Y. Liu, Relationship between Pd oxidation states on TiO_2 and the photocatalytic oxidation behaviors of nitric oxide, Chemosphere 77 (2009) 264–268.
[60] S. Goldstein, G. Czapski, Direct and indirect oxidations by peroxynitrite, Inorg. Chem. 34 (1995) 4041–4048.
[61] W.A. Pryor, G.L. Squadrito, The chemistry of peroxynitrite: a product from the reaction of nitric oxide with superoxide, Am. J. Physiol. Lung Cell. Mol. Physiol. 268 (1995) L699–L722.
[62] J.W. Coddington, J.K. Hurst, S.V. Lymar, Hydroxyl radical formation during peroxynitrous acid decomposition, J. Am. Chem. Soc. 121 (1999) 2438–2443.
[63] G. Merényi, J. Lind, Free radical formation in the peroxynitrous acid (ONOOH)/Peroxynitrite ($ONOO^-$) system, Chem. Res. Toxicol. 11 (1998) 243–246.
[64] R.J. Gustafsson, A. Orlov, P.T. Griffiths, R.A. Cox, R.M. Lambert, Reduction of NO_2 to nitrous acid on illuminated titanium dioxide aerosol surfaces: implications for photocatalysis and atmospheric chemistry, Chem. Commun. (2006) 3936–3938.
[65] M. Ammann, R.A. Cox, J.N. Crowley, M.E. Jenkin, A. Mellouki, M.J. Rossi, J. Troe, T.J. Wallington, Evaluated kinetic and photochemical data for atmospheric chemistry: volume VI – heterogeneous reactions with liquid substrates, Atmos. Chem. Phys. 13 (2013) 8045–8228.
[66] R. Atkinson, D.L. Baulch, R.A. Cox, J.N. Crowley, R.F. Hampson, R.G. Hynes, M.E. Jenkin, M.J. Rossi, J. Troe, Evaluated kinetic and photochemical data for atmospheric chemistry: volume I – gas phase reactions of O_x, HO_x, NO_x and SO_x species, Atmos. Chem. Phys. 4 (2004) 1461–1738.
[67] R. Atkinson, D.L. Baulch, R.A. Cox, J.N. Crowley, R.F. Hampson, R.G. Hynes, M.E. Jenkin, M.J. Rossi, J. Troe, Evaluated kinetic and photochemical data for atmospheric chemistry: volume III– gas phase reactions of inorganic halogens, Atmos. Chem. Phys. 7 (2007) 981–1191.
[68] R. Atkinson, D.L. Baulch, R.A. Cox, J.N. Crowley, R.F. Hampson, R.G. Hynes, M.E. Jenkin, M.J. Rossi, J. Troe, Evaluated kinetic and photochemical data for atmospheric chemistry: volume II– gas phase reactions of organic species, Atmos. Chem. Phys. 6 (2006) 3625–4055.
[69] R. Atkinson, D.L. Baulch, R.A. Cox, J.N. Crowley, R.F. Hampson, R.G. Hynes, M.E. Jenkin, M.J. Rossi, J. Troe, T.J. Wallington, Evaluated kinetic and photochemical data for atmospheric chemistry: volume IV – gas phase reactions of organic halogen species, Atmos. Chem. Phys. 8 (2008) 4141–4496.
[70] J.N. Crowley, M. Ammann, R.A. Cox, R.G. Hynes, M.E. Jenkin, A. Mellouki, M.J. Rossi, J. Troe, T.J. Wallington, Evaluated kinetic and photochemical data for atmospheric chemistry: volume V – heterogeneous reactions on solid substrates, Atmos. Chem. Phys. 10 (2010) 9059–9223.
[71] J.N. Crowley, M. Ammann, R.A. Cox, R.G. Hynes, M.E. Jenkin, A. Mellouki, M.J. Rossi, J. Troe, T.J. Wallington, Corrigendum to "Evaluated kinetic and photochemical data for atmospheric chemistry: volume V – heterogeneous reactions on solid substrates" published in Atmos. Chem. Phys. 10, 9059–9223, 2010, Atmos. Chem. Phys. 13 (2013) 7359.
[72] NDRL/NIST Solution Kinetics Database Version 3.0, National Institute of Standards and Technology, Gaithersburg, 1998.
[73] J. Ângelo, L. Andrade, L.M. Madeira, A. Mendes, An overview of photocatalysis phenomena applied to NO_x abatement, J. Environ. Manage. 129 (2013) 522–539.
[74] S. Devahasdin, C. Fan Jr., K. Li, D.H. Chen, TiO_2 photocatalytic oxidation of nitric oxide: transient behavior and reaction kinetics, J. Photochem. Photobiol. A Chem. 156 (2003) 161–170.
[75] R. Dillert, J. Stötzner, A. Engel, D.W. Bahnemann, Influence of inlet concentration and light intensity on the photocatalytic oxidation of nitrogen(II) oxide at the surface of Aeroxide® TiO2 P25, J. Hazard. Mater. 211–212 (2012) 240–246.
[76] A. El Zein, Y. Bedjanian, Interaction of NO_2 with TiO_2 surface under UV irradiation: measurements of the uptake coefficient, Atmos. Chem. Phys. 12 (2012) 1013–1020.
[77] G. Hüsken, M. Hunger, H.J.H. Brouwers, Experimental study of photocatalytic concrete products for air purification, Build. Environ. 44 (2009) 2463–2474.
[78] A.R. Jayapalan, B.Y. Lee, E.M. Land, M.H. Bergin, K.E. Kurtis, Photocatalytic efficiency of cement-based materials: demonstration of proposed test method, ACI Mater. J. 112 (2015) 219–228.
[79] S.S. Lucas, V.M. Ferreira, J.L.B. de Aguiar, Incorporation of titanium dioxide nanoparticles in mortars — influence of microstructure in the hardened state properties and photocatalytic activity, Cem. Concr. Res. 43 (2013) 112–120.
[80] Y. Murata, H. Tawara, H. Obata, K. Takeuchi, Air purifying pavement: development of photocatalytic concrete blocks, J. Adv. Oxid. Technol. 4 (1999) 227–230.
[81] H. Wang, Z. Wu, W. Zhao, B. Guan, Photocatalytic oxidation of nitrogen oxides using TiO_2 loading on woven glass fabric, Chemosphere 66 (2007) 185–190.
[82] A.V. Emeline, V.K. Ryabchuk, N. Serpone, Dogmas and misconceptions in heterogeneous photocatalysis. Some Enlightened Reflections, J. Phys. Chem. B 109 (2005) 18515–18521.
[83] A. Engel, J. Große, R. Dillert, D.W. Bahnemann, The influence of irradiance and humidity on the photocatalytic conversion of nitrogen(II) oxide, J. Adv. Oxid. Technol. 18 (2015) 195–203.
[84] M. Hunger, G. Hüsken, H.J.H. Brouwers, Photocatalytic degradation of air pollutants - from modeling to large scale application, Cem. Concr. Res. 40 (2010) 313–320.
[85] J.V.S. de Melo, G. Trichês, Evaluation of the influence of environmental conditions on the efficiency of photocatalytic coatings in the degradation of nitrogen oxides (NO_x), Build. Environ. 49 (2012) 117–123.
[86] H. Ichiura, T. Kitaoka, H. Tanaka, Photocatalytic oxidation of NO_x using composite sheets containing TiO_2 and a metal compound, Chemosphere 51 (2003) 855–860.
[87] Y. Ohko, Y. Nakamura, N. Negishi, S. Matsuzawa, K. Takeuchi, Unexpected release of HNO_3 and related species from UV-illuminated TiO_2 surface into air in photocatalytic oxidation of NO_2, Environ. Chem. Lett. 8 (2009) 289–294.
[88] VDI 3782, Part 5. Environmental Meteorology, Atmospheric Dispersion Models, Deposition Parameters, VDI/DIN-Handbuch Reinhaltung der Luft, Band 1b, (2006).
[89] A. Engel, A. Glyk, A. Hülsewig, J. Große, R. Dillert, D.W. Bahnemann, Determination of the photocatalytic deposition velocity, Chem. Eng. J. 261 (2015) 88–94.